ACS OMEGA

http://pubs.acs.org/journal/acsodf

Article

Nanocomposite of Ceria and Trititanate Nanotubes as an Efficient Defluoridating Material for Real-Time Groundwater: Synthesis, Regeneration, and Leached Metal Risk Assessment

Anjana Biswas and Prathibha C*

Cite This: *ACS Omega* 2021, 6, 31751−31764

Read Online

ACCESS | Metrics & More | Article Recommendations | Supporting Information

ABSTRACT: Ceria-incorporated trititanate nanotube composite (CTNC) was synthesized via a simple two-step wet chemical route for efficient fluoride removal not only from synthetic water but also from groundwater. The synthesized nanomaterial was systematically characterized for its physical and chemical properties. CTNC was shown to be highly porous with a surface area of 267 m^2/g. The high surface area exposed majority of its adsorption sites, that is, surface hydroxyl groups, for fluoride removal. The plausible adsorption mechanism deduced based on FTIR and XPS data showed that ion exchange between the surface hydroxyl groups and the fluoride ions in water played a vital role in defluoridation by CTNC. A novel approach was used to quantify the adsorption sites with the use of BET and thermogravimetric analysis. TEM images confirmed the morphology of CTNC to be nanotubes decorated with ceria particles. The analysis of treated water samples for the metal ion content was carried out by an ICP-MS technique. CTNC exhibited characteristics of an ideal adsorbent such as high adsorption capacity, faster kinetics, pH independent adsorption, good regeneration, and negligible leaching of metal ions into the effluent. These attractive characteristics enabled the applicability of CTNC for real-time use.

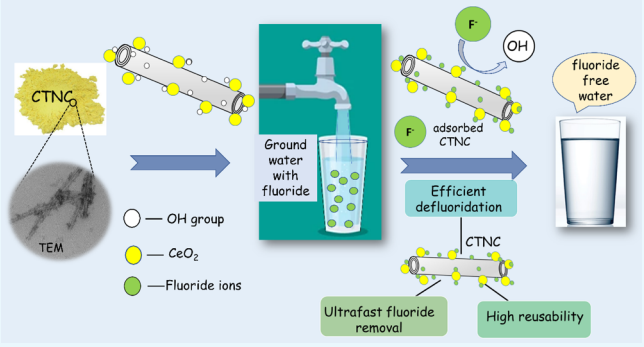

1. INTRODUCTION

Groundwater is the primary water source that meets about 85% of the drinking and other domestic water needs. However, the presence of various contaminants in groundwater is a major cause of concern across the globe. Fluoride is one such harmful contaminant. According to the World Health Organization (WHO), the presence of fluoride in water in concentrations above 1.5 mg/L has detrimental effects on human health.[1] The Bureau of Indian Standards (BIS) has set the safe limit of fluoride in drinking water to be 1 mg/L.[2] The hazardous impact includes dental and skeletal fluorosis; prolonged exposure to high levels of fluoride in water also causes neurological disorders, infertility, thyroid issues, and even cancer.[1,3] Fluoride contamination is a global problem affecting more than 260 million people across 25 countries including India.[3] Considering the scenario in India, as per Central Ground water board, Government of India, 225 districts in the 19 states of India are affected by fluoride contamination.[4] Therefore, it is of utmost importance that fluoride is removed from water before it is consumed. Researchers have been working towards this direction with the intention of developing efficient fluoride removal techniques. This has resulted in a variety of water defluoridation technologies: precipitation and coagulation, reverse osmosis, ion exchange, nanofiltration, and adsorption.[5]

Among the methods mentioned, adsorption is most effective due to its diverse advantages that include ease of operation, good efficiency, low cost, and high reusability.[5,6] However, the success of the adsorption process is determined by adsorbent properties. The ideal properties of any adsorbent must include efficient adsorption of fluoride in a very short span of time using minimal quantities of adsorbents. There are a variety of adsorbents reported in the literature, which include ion exchange resins,[7] bio-adsorbents,[8] clay,[9] alum sludge,[10] soil,[11] zeolites,[12] and activated carbon.[13] However, they have limited use due to either poor efficiency, slow kinetics, or a need for large quantities of adsorbents. The properties necessary for an efficient adsorbent are easily obtained in nanomaterials due to their exceptional properties, majorly their high surface area and small size. Since adsorption is a surface phenomenon, a higher adsorbent surface area implies that majority of the active adsorbent sites are on the adsorbent surface and readily available for fluoride adsorption. Therefore, efficient adsorp-

Received: August 16, 2021
Accepted: October 21, 2021
Published: November 16, 2021

tion can take place rapidly using a very small quantity of nano-adsorbents.

It has been reported that several metal oxide nanoparticles have efficient fluoride removal capacity; these include oxides of La(III), Zr(IV), Ce(IV), and Ti(IV).[14] Adsorbents based on titania are versatile and nontoxic and have high affinity for fluoride.[6,15] Oxides of cerium have also been explored for fluoride removal, revealing its good affinity for anionic contaminants like fluoride.[16] However, many of these materials are not useful in treating groundwater as they are either pH dependent or they do not have fast kinetics or they have poor selectivity for fluoride in the presence of other ions or their adsorption sites cannot be regenerated. Hence, many studies do not report the field trials. For instance, the recent work on GO-CeO_2[17] does not report any study on applicability of the material in defluoridating groundwater as the material is pH sensitive and possesses low fluoride removal efficiency at neutral pH, though it exhibits faster kinetics. This limits the application of these materials from being translated into real-time fluoride filters. Therefore, the search for a fluoride adsorbent that works for real-time conditions continues. In the current work, the authors present the material ceria-incorporated trititanate nanotube composite (CTNC) that has been suitably developed to work for this real-time application. This work is a systematic report on the synthesis and characterization of CTNC, along with the detailed assessment of its fluoride removal efficiency not only from synthetic water in the laboratory but also from real-time groundwater samples. To the best of our knowledge, this material has not been explored before for the removal of contaminants from groundwater. This is the first report of application of CTNC in remediating fluoride from groundwater.

The material properties of the as-synthesized adsorbent were thoroughly investigated and analyzed using XRD, SEM−EDX, TEM, BET, TGA, FTIR, and XPS. Batch adsorption studies were carried out to optimize the effect of pH, contact time, adsorbent dosage, initial fluoride concentration, competing ions, and regeneration capacity. The material presented here is a potential adsorbent with abundance of adsorption sites. The number of these active adsorption sites per gram of the adsorbent has been quantified to understand their effect on fluoride adsorption. A detailed discussion on the probable adsorption mechanism is also presented. This material is easy to synthesize and exhibits ultrafast removal of fluoride ions, with very high fluoride removal efficiency. The applicability of the material for defluoridating water was thoroughly investigated with real-time groundwater samples collected from different areas in Anantapur district, Andhra Pradesh, India, where the authors' university is situated. The robustness of the adsorbent and risk of metal ion leaching from the adsorbent along with its regeneration capacity while defluoridating groundwater were also estimated.

2. RESULTS AND DISCUSSION

2.1. Adsorbent Synthesis and Optimization. The solubility of the salt ceric ammonium nitrate (CAN) in water is very high. Pettinger et al. reported in their work[18] that cerium oxide (or Ceria) nanoparticles are formed spontaneously at room temperature when CAN is dissolved in water. CAN being a strong Lewis acid, the pH of the solution reduces to ∼2, upon dissolution in water. This rapid drop in pH, which occurred due to hydrolysis of CAN in water, was the driving force for the formation of ceria nanoparticles. When HTNT (hydrogen titanate nanotubes) was introduced into the CAN solution and magnetically stirred for a long period of time, two processes take place, that is, decoration of the ceria nanoparticles on the HTNT surface and ion exchange between Ce ions from the solution with the hydrogen ions in the interlayer region of layered titanate nanotube structure. The arrangement of ceria nanoparticles on the nanotube surface takes place via electrostatic interaction.[19−21] Further, post filtration, when the product was heated to 80 °C, the CeO_2 nanoparticles bound themselves effectively on the HTNT surface. This led to the formation of ceria-incorporated trititanate nanotube composite (CTNC).

The as-synthesized CTNC, which was initially air-dried at 80 °C, was next calcined for 2 h to different temperatures: 150 to 500 °C in steps of 50 °C. This was performed in order to study the effect of calcination temperature on adsorbent efficiency, thereby optimizing the sample that would be used for further studies. As shown in Figure 1, there was a significant

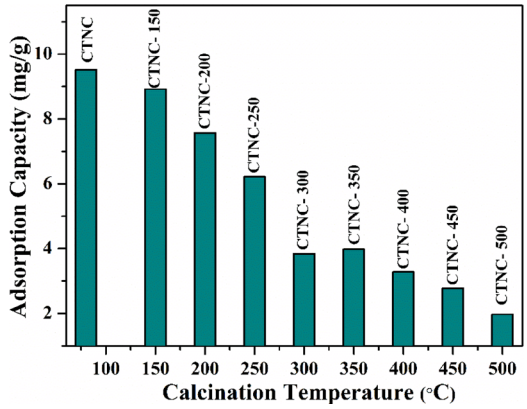

Figure 1. Effect of calcination temperature on fluoride adsorption capacity with 1 g/L adsorbent and 10 mg/L fluoride at pH 7 for 30 min.

decrease in the adsorption capacity with the increase in calcination temperatures. Upon heat treatment, the following events might take place: destruction of the nanotubular morphology; sharp decrease in the number of surface hydroxyl groups on the adsorbent surface; and decomposition of the $H_2Ti_3O_7$ phase to TiO_2.[6,22,23] The combined effect of these events resulted in the decrease in adsorption capacity upon heating. Hence, CTNC dried at 80 °C was used for further physicochemical and adsorption experiments.

2.2. Adsorbent Characterization. *2.2.1. Phase and Morphology.* The XRD pattern of the pristine adsorbent is shown in Figure 2a, which consists of peaks at 2θ = 9.5, 24.4, 28.3, 32.6, 48.4, 56.9, 70.4, and 78.1°. The peaks at 9.5, 24.4, 28.4, and 48.4° assigned to the (*hkl*) planes (200), (110), (310), and (020), respectively, could be attributed to the monoclinic phase of HTNT with space group *C*2/*m*. The results are further in agreement with the ICSD # 98-023-7518 and previous literature reports.[24−27] The peaks at 28.4, 32.6, 48.4, 56.7, 70.4, and 78.1° correspond to the planes (111), (200), (220), (311), (400), and (331) respectively, and represent the face-centered cubic phase of CeO_2 with space group $Fm\bar{3}m$.[16,28,29] This is also in accordance with the data in ICSD # 98-019-2225. It can be observed that the peaks at 28.4 and 48.4° correspond to both the phases of HTNT and CeO_2.

https://doi.org/10.1021/acsomega.1c04424
ACS Omega 2021, 6, 31751−31764

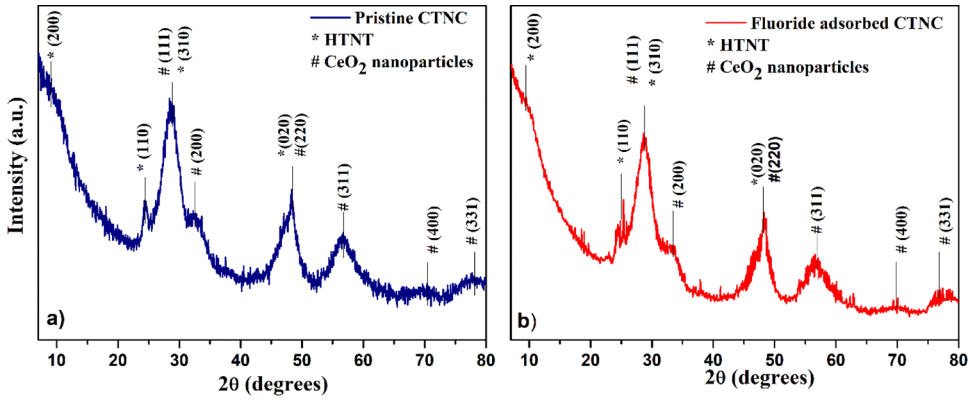

Figure 2. XRD of (a) pristine adsorbent CTNC and (b) fluoride adsorbed CTNC.

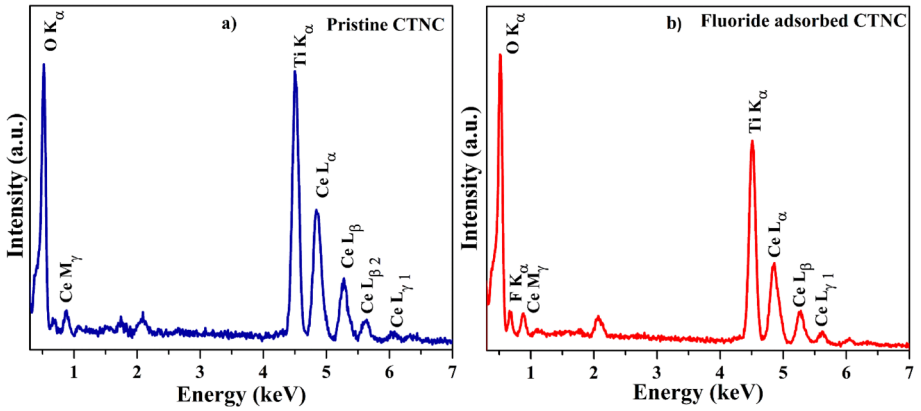

Figure 3. EDX spectra of (a) pristine CTNC and (b) fluoride adsorbed CTNC.

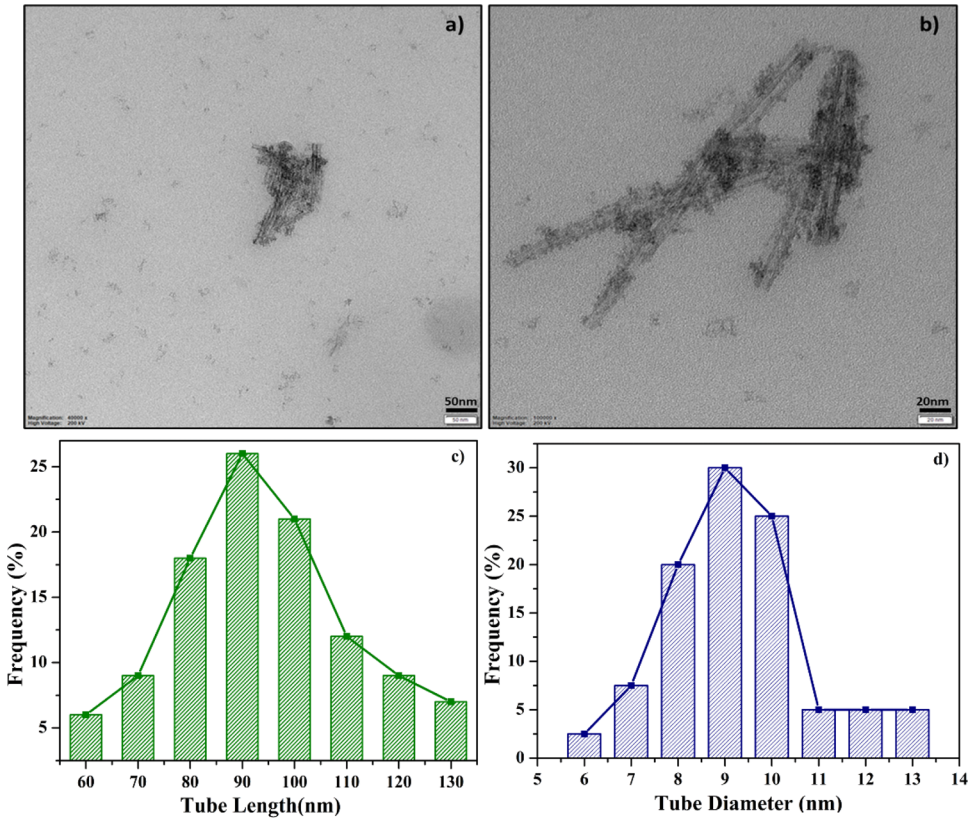

Figure 4. (a, b) TEM images of CTNC, (c) tube length distribution, and (d) tube diameter distribution

https://doi.org/10.1021/acsomega.1c04424
ACS Omega 2021, 6, 31751−31764

The intensities of these two peaks result from both the phases. The XRD results therefore indicate that the as-synthesized adsorbent, CTNC, is composed of both the distinct phases of HTNT and ceria. Hence, it proved the successful formation of a material that is a composite of ceria and titanate nanotubes.

Figure 2b shows the XRD pattern of CTNC post fluoride adsorption. The fluoride adsorbed CTNC had the same eight peaks as the pristine adsorbent without any new peak, but with a slight shift in peak positions (9.5, 24.8, 28.9, 33.1, 48.4, 56.9, 70.5, and 78.3°). This slight shift in positions was possibly due to successful binding of fluoride with the CTNC surface.

The elemental composition of CTNC was estimated by mapping the scanned surface at multiple positions using energy-dispersive X-ray spectroscopy. The EDX spectra of pristine CTNC and fluoride adsorbed CTNC are shown in Figure 3. The EDX spectra of CTNC consist of peaks corresponding to the elements Ti, Ce, and O. The atomic percentage compositions of CTNC were as follows: Ti − 16.22%, Ce − 7.02%, and O − 76.75%. The absence of any impurity peak confirms the purity of the product. The EDX map of fluoride adsorbed CTNC, as shown in Figure 3b, consists of an additional peak corresponding to F K_{α}, which proves the successful uptake of fluoride ions by CTNC. The atomic percentage of the fluoride present in fluoride adsorbed CTNC is 2.2%. The elemental maps of pristine CTNC and fluoride adsorbed CTNC are shown in Figures S1 and S2. The maps show the uniform distribution of the elements on the adsorbent surface.

The morphology of the nanocomposite was confirmed using transmission electron microscopy (TEM). Figure 4 shows the TEM images of CTNC. It can be clearly observed that the adsorbent consists of bundles of particles that are tubular in shape with small spherical particles on their surface. These nanotubes correspond to the titanate phase. The randomly aligned nanotubes have lengths in the range 60−135 nm and outer diameters of 7−12 nm. The average length of the nanotubes was 95 nm, whereas the average diameter was 9 nm. The size distribution for the same material is shown in Figure 4c,d. In addition, spherical nanoparticles present on the surface of nanotubes correspond to ceria. Thus, it could be concluded that the CTNC morphology consists of bundles of nanotubes of trititanate decorated with spherical ceria particles on its surface. Further, the incorporation of the ceria nanoparticles did not disturb the tubular morphology of the parent material HTNT.

2.2.2. Surface Area. The specific surface area of CTNC was measured using the Brunauer−Emmett−Teller (BET) method of surface area analysis. As shown in Figure 5, the N_2 adsorption and desorption curves do not retrace each other, thus giving rise to a hysteresis loop. This pattern corresponds to the IUPAC type IV BET isotherm. The presence of hysteresis implies that the adsorbent has a mesoporous structure. The specific surface area (SSA) of the as-synthesized nanocomposite was estimated to be 267 m^2/g. The average pore size was estimated with the BJH method. The average pore radius and pore volume for CTNC were 5.6 nm and 0.586 cc/g, respectively. The pore size of CTNC further indicates that these pores are readily accessible for fluoride ion adsorption (ionic radius of fluoride ions: 0.133 nm). The SSA for the parent HTNT was measured to be 235 m^2/g[16,29] for the adsorption process, which is a surface phenomenon. With its high SSA and small pore size, CTNC presents majority of active adsorption sites available on the surface, which will result in enhanced fluoride removal.

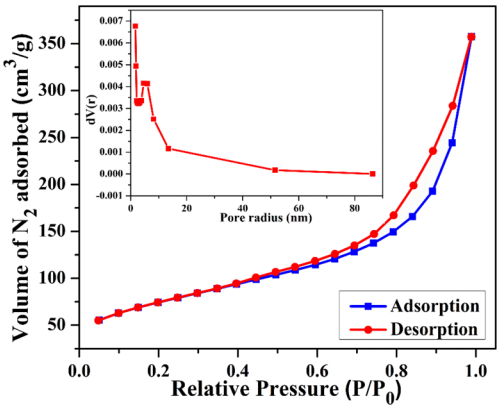

Figure 5. N_2 adsorption−desorption curves and BJH pore size distribution for CTNC

2.3. Batch Adsorption Process. It is important to optimize the operating parameters affecting the fluoride adsorption process to obtain maximum adsorption efficiency from the adsorbent. The adsorption capacity of any adsorbent is majorly affected by the initial pH of the solution, the time for which the adsorbent is in contact with water, initial fluoride concentration, adsorbent dosage, and co-existing competitive ions. Further it is important to evaluate the regeneration capacity of the adsorbent to ensure that it is cost-effective for real-time use. The effect of these parameters on fluoride adsorption capacity of CTNC was studied through a batch adsorption process.

2.3.1. pH Studies. The effect of solution pH on fluoride adsorption was studied by subjecting 1 g/L CTNC to 10 mg/L fluoride solutions pre-adjusted to different pH levels of 2−9, with the contact time maintained at 30 min. The pH of solutions was adjusted using 0.1 M HCl and 0.1 M NaOH. As shown in Figure 6a, the adsorption capacity and hence the percentage fluoride adsorption of CTNC were almost unaffected with the variation of the initial pH of the fluoride-containing aqueous solution. Thus, it could be said that CTNC exhibited a very wide pH window for fluoride adsorption, which is an ideal characteristic of a good adsorbent.

A maximum of 96.4% fluoride adsorption was obtained at pH 3, after which there was a very slow decrease in the adsorption percentage to 85.5% at pH 9. Under neutral pH conditions, 90.1% of fluoride removal was obtained and the fluoride concentration in the effluent was ≤1 mg/L, which is within the permissible limits of WHO and BIS.

During the investigation of the effect of initial pH on adsorption capacity of CTNC, it was also observed that the pH of the solution underwent a change after fluoride adsorption. This change in solution pH post fluoride adsorption ($\Delta pH = pH_f - pH_i$) as a function of the initial pH (pH_i) of the solution is shown in Figure 6b. As seen from the figure, post fluoride adsorption at pH 7, the change in solution pH was negligible. Therefore, CTNC leaves the defluoridated water with permissible fluoride and pH, making it potable.

2.3.2. Kinetics of Adsorption in CTNC. The adsorption of fluoride is greatly affected by the contact time between the adsorbent and fluoride-contaminated water. CTNC (1 g/L) was added to 10 mg/L fluoride solutions at pH 7, and adsorption experiments were carried out for 1−120 min.

https://doi.org/10.1021/acsomega.1c04424
ACS Omega 2021, 6, 31751−31764

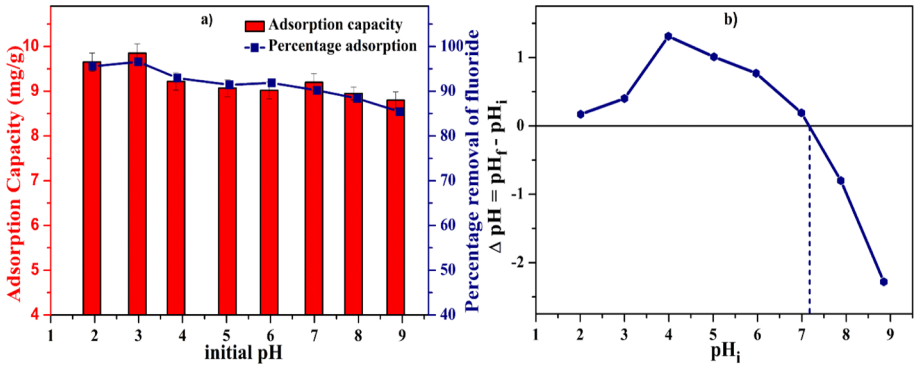

Figure 6. (a) Variation of adsorption capacity and percentage adsorption with the initial pH of the solution (adsorbent dosage: 1 g/L, contact time: 30 min, initial fluoride concentration: 10 mg/L). (b) Change in the solution pH as a function of initial pH during fluoride adsorption.

CTNC exhibited a rapid fluoride adsorption (Figure 7). It is interesting to note that CTNC could remove majority of the

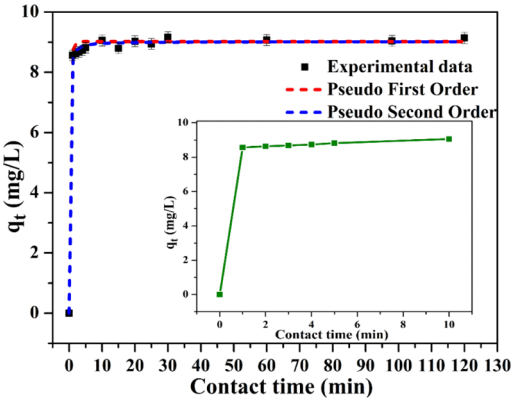

Figure 7. Variation of adsorption capacity with the contact time (pH 7, adsorbent dosage: 1 g/L, initial fluoride concentration: 10 mg/L); pseudo-first-order and pseudo-second-order kinetics fit of the data

fluoride ions within just 1 min of contact time, and the adsorption capacity continued to increase slightly till 10 min, after which it equilibrates. Thus, most of the fluoride ions were adsorbed by CTNC almost instantaneously. This ultrafast fluoride adsorption could be attributed to the abundance of hydroxyl groups readily available on the surface of CTNC. This could be due to the tubular morphology, intercalation of the Ce ions, large number of nanoparticles decorated on the tubes, and high surface area, which ensure the maximum availability of the adsorption sites on the adsorbent surface. The adsorption kinetics of CTNC was much faster than that of previously reported ceria nanoparticles and HTNT. Dhillon et al.[16] reported that for ceria nanoparticles, the fluoride adsorption was rapid in the first 1 h and it equilibrated in 2 h. Further, Chinnakoti et al.[6] reported in their work that HTNT exhibited rapid adsorption in the first 10 min of contact time, which reached equilibrium in 2 h. Therefore, the time taken to reach equilibrium fluoride adsorption using CTNC was 12 times faster than that of both HTNT and ceria nanoparticles.

This data was further analyzed with the help of two common kinetic models: pseudo-first-order (PFO) and pseudo-second-order (PSO) kinetic models, which could be represented by eqs E.1 and E.2, respectively, as shown below:

$$q_t = q_e(1 - e^{-k_1 t}) \quad \text{(E.1)}$$

$$q_t = \frac{k_2 q_e^{\,2} t}{1 + k_2 q_e t} \quad \text{(E.2)}$$

where q_e is the equilibrium fluoride adsorption capacity in mg/g, q_t is the fluoride adsorption capacity at time t in mg/L, k_1 (1/min) is the PFO equilibrium rate constant, and k_2 (g/mg·min) is the PSO equilibrium rate constant. The parameters calculated from fitting the experimental data with these models are tabulated in Table 1.

It could be seen that both the models, PFO and PSO, fit the data well with an R^2 value ~1. Further, in both the cases, the calculated values of equilibrium adsorption capacity, $q_{e,cal}$, were 9.06 mg/g for PFO and 9.02 mg/g for the PSO kinetic model, which were in agreement with the experimentally determined value. Hence, the χ^2 test was used to identify the model that fit the data better. The χ^2 value for PSO was 0.0091, which was lesser than that of PFO. Therefore, the pseudo-second-order model was a better model to describe the kinetics of CTNC. Hence, the rate-limiting step in the fluoride adsorption kinetics of CTNC might depend on valence forces through sharing or exchange of electrons and the number of available adsorption sites.[6,16,31]

2.3.3. Adsorption Isotherms. The fluoride adsorption capacity of any adsorbent depends on the initial fluoride concentration. The adsorption experiments were conducted with different fluoride concentrations from 3 to 165 mg/L at pH 7, with an adsorbent dosage of 1 g/L and a contact time of 30 min. It was observed that the adsorption capacity increased with the increase in initial fluoride conditions. This indicated that a large number of active sites were available on the CTNC

Table 1. Parameters Calculated from Adsorption Kinetics Studies

	pseudo-first-order parameters				pseudo-second-order parameters			
$q_{e,exp}$ (mg/g)	k_1 (min^{-1})	$q_{e,cal}$ (mg/g)	R^2	χ^2	k_2 (g/mg min)	$q_{e,cal}$ (mg/g)	R^2	χ^2
9.07	2.89	9.06	0.9934	0.0114	1.57	9.02	0.9976	0.0091

https://doi.org/10.1021/acsomega.1c04424
ACS Omega 2021, 6, 31751−31764

surface, which made it an efficient fluoride adsorbent at both low and high concentrations of fluoride.

Figure 8 shows the variation of fluoride adsorption capacity with the equilibrium fluoride concentration. This study could

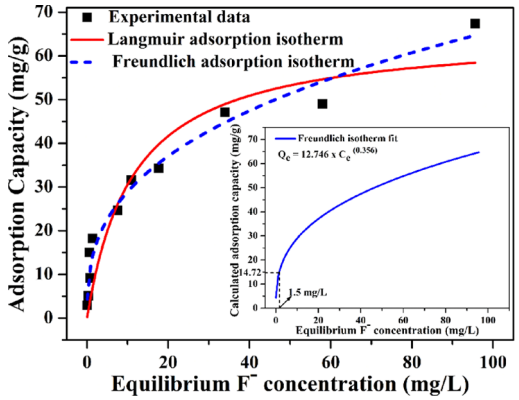

Figure 8. Variation of adsorption capacity with the equilibrium fluoride concentration (pH 7, adsorbent dosage: 1 g/L, contact time: 30 min); Langmuir and Freundlich isotherm fit of the data.

further be utilized to analyze the nature of interaction between the adsorbent (CTNC) and the adsorbate (fluoride ions) and also quantify the maximum adsorption capacity. This was done by fitting the data to two common adsorption isotherm models: Langmuir isotherm and Freundlich isotherm.

The Langmuir adsorption isotherm[32] assumes monolayer adsorption on the homogenous adsorbent surface, where there is no interaction between the adsorbate and adsorbent. It could be mathematically represented as given in eq E.3

$$q_e = q_{max} b c_e / (1 + b c_e) \quad \text{(E.3)}$$

where q_e (mg/g) is the equilibrium adsorption capacity, c_e (mg/L) is the equilibrium fluoride concentration, b (L/mg) is the Langmuir isotherm constant, and q_{max} (mg/g) is the theoretical maximum fluoride adsorption capacity.

The Freundlich adsorption isotherm[33] assumes heterogeneous adsorption sites while considering lateral interaction between the adsorbent and adsorbate. This adsorption isotherm is given by eq E.4

$$q_e = K_f c_e^{1/n} \quad \text{(E.4)}$$

where K_f ((mg/g) $(L/mg)^{1/n}$) is the Freundlich isotherm constant and $(1/n)$ is a heterogeneity factor indicative of the adsorption intensity.

It was observed that the Freundlich adsorption isotherm with R^2 = 0.97 isotherm offers a better fit to the adsorption data of CTNC than the Langmuir isotherm with R^2 = 0.88. The value of the heterogeneity factor, n, from the Freundlich isotherm was calculated to be 2.807, which was in the range $1 < n < 10$, indicating favorable adsorption. From the Langmuir isotherm fit, the theoretical maximum monolayer adsorption capacity (q_{max}) was calculated to be 65.37 mg/g. Under room temperature conditions, this value is higher compared to that of CeO_2 nanoparticles.[16] Further, pure HTNT had negligible fluoride adsorption at pH 7,[6] thus proving the enhancement in the adsorption capacity in the composite material compared to their individual counterparts. The comparison of this value with other reported adsorbents is tabulated in Table 5.

The WHO standard for fluoride in drinking water is as low as 1.5 mg/L, that is, $c_e \leq 1.5$ mg/L. Therefore, it is important to determine the adsorption capacity of CTNC at this low fluoride concentration. This was done using the Freundlich fit of the experimental adsorption data, as shown in Figure 8. It was observed that at c_e = 1.5 mg/L, the fluoride adsorption capacity of CTNC was 14.72 mg/g. This value indicated that CTNC could act as a very good fluoride adsorbent to remediate contaminated water to the WHO limits. The parameters calculated from the two adsorption isotherms are tabulated in Table 2. The isotherms also indicate the possibility of the mechanism of fluoride adsorption to be both combination of physisorption and chemisorption.

Table 2. Parameters Calculated from the Adsorption Isotherms

Langmuir isotherm			Freundlich isotherm		
q_{max} (mg/g)	b (L/g)	R^2	K_f (mg/g)(L/mg)$^{(1/n)}$	N	R^2
65.37	0.088	0.88	12.75	2.807	0.97

2.3.4. Adsorption Mechanism. It is essential to understand the mechanism of fluoride adsorption by the adsorbent in order to improvise its efficiency. The hydrolysis of metal oxides in water leads to the formation of surface hydroxyl groups.[14] These M−OH groups are present in abundance on metal oxides and are considered to be the most important active sites for anion adsorption from water. The presence of M−OH groups on the adsorbent surface was qualitatively shown by FTIR and XPS analysis. We report a novel approach to quantify these groups on the adsorbent surface based on BET and TGA data. The significance of hydroxyl groups in the fluoride adsorption mechanism of CTNC was thoroughly investigated and analyzed using the FTIR and XPS spectroscopic techniques.

2.3.4.1. Quantification of Adsorption Sites and Surface Hydroxyl Groups. In combination with BET specific surface area analysis, thermogravimetric analysis (TGA) was used to quantify the number of surface hydroxyl groups present on the surface of CTNC. Though a similar analysis has been reported,[34−36] there are very few reports where the number of these active adsorption sites, that is, the surface hydroxyl groups, have been quantified for fluoride adsorbents.

Thermogravimetric analysis was carried out by heating CTNC initially from room temperature to 120 °C at 10 °C/min. This is shown by step I in Figure 9, which represents the thermogram of CTNC. The sample was held isothermal at this temperature for 10 min in order to remove any water molecules physically adsorbed on the sample surface due to atmospheric humidity. Further, the sample was heated from 120 to 600 °C at a rate of 10 °C/min. According to Mueller et al., the surface of the material based on titania is considered to be free of surface hydroxyl groups at 500 °C.[35] Therefore, as shown in step II in Figure 9, the weight loss of 9.19% undergone by CTNC when it was heated from 120 to 500 °C corresponds to the loss of surface hydroxyl groups. This value was further used to estimate the number of surface hydroxyl groups of CTNC using the following formula:

https://doi.org/10.1021/acsomega.1c04424
ACS Omega 2021, 6, 31751−31764

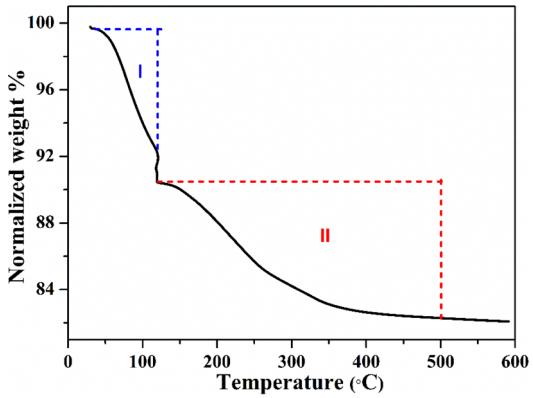

Figure 9. TGA curve of CTNC.

$$\#\mathrm{OH/nm^2} = \alpha \frac{(\text{number of OH/nm}^2)_{T_2} \times \mathrm{SSA} \times W_{T_2} + \left[\frac{(W_{T_1} - W_{T_2})}{\frac{\mathrm{MW_{H_2O}}}{N_A}} \times 2\right]}{\mathrm{SSA} \times W_{T_1}} \quad \text{(E.5)}$$

where W_{T_1} and W_{T_2} are the weights of the sample at temperatures T_1 and T_2, respectively, SSA is the specific surface area (nm^2/g) as measured from the BET studies, $\#OH/nm^2$ represents the number of surface hydroxyl groups per nm^2 of the sample surface, MW_{H_2O} is the weight of the water molecules, α is the calibration factor equal to 0.625, and N_A is the Avogadro's number. OH content per gram of the material is finally calculated as $\#OH/nm^2 \times SSA$. In this study, T_1 was 120 °C, where the physiosorbed water molecules (absorbed atmospheric moisture) leave the adsorbent surface; T_2 was 500 °C at which titania-based materials lose all their surface hydroxyl groups.

The study revealed that CTNC with an SSA of 267 m^2/g had 16.55 OH groups per nm^2 of sample surface. This further implies that 1 g of CTNC effectively has 4.42×10^{21} OH groups on its surface. This quantification confirmed the abundant availability of surface hydroxyl groups on the CTNC surface. Further, this value is ∼14 times higher than the number of fluoride ions present in 10 mg/L fluoride-containing water. Therefore, the CTNC surface has plenty of adsorption sites to undergo ion exchange with the fluoride ions from water, leading to highly efficient fluoride adsorption.

2.3.4.2. FTIR. The fluoride adsorption mechanism of CTNC was further studied with the help of FTIR analysis of the pristine and fluoride adsorbed CTNC. As depicted in Figure 10, the pure CTNC consists of a broad peak positioned at 3269 cm^{-1} and a sharp peak at 1639 cm^{-1}, which could be attributed to the stretching and bending vibrations of H−OH and −OH groups of metal oxide and adsorbed water.[21] The sharp peak at 1033 cm^{-1} corresponds to the bending vibrations of M−OH (where M = Ce and Ti) present in CTNC, which disappeared post fluoride adsorption.

The peaks at 1456 and 655 cm^{-1} could be assigned to M−O (M = Ce and Ti). These results are consistent with the previously reported literature.[16,23,37] Post fluoride adsorption, the peak at 3269 cm^{-1}, corresponding to the −OH stretch in the pristine adsorbent, shifted to 3297 cm^{-1} with reduced intensity. The intensity of the peaks of M−OH reduced considerably or disappeared in the spectra obtained for fluoride

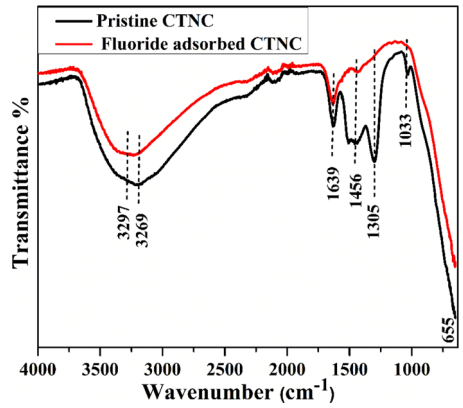

Figure 10. FTIR spectra of pristine and fluoride adsorbed CTNC.

adsorbed CTNC. This was due to the successful exchange of the hydroxyl ions with fluoride ions in water, thus indicating the possibility of an ion exchange mechanism in CTNC.[5,6,30]

2.3.4.3. XPS. To further validate the ion exchange mechanism, elemental analysis was carried out using X-ray photoelectron spectroscopy of pristine and fluoride adsorbed CTNC. The XPS spectra were corrected to the binding energy of adventitious carbon, 284.6 eV. Further, the peaks were fitted to Gaussian−Lorentzian curves with Shirley background using the software XPS peak41.

The wide-angle survey spectra of CTNC, as shown in Figure 11, consisted of peaks corresponding to Ti 2p, O 1s, and Ce

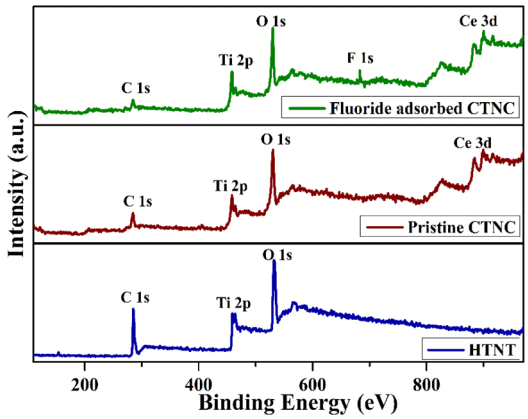

Figure 11. Survey spectra of HTNT, CTNC, and F adsorbed CTNC.

3d. The presence of Ce 3d in CTNC, which was initially absent in the parent HTNT, proves the successful incorporation of Ce in the adsorbent. This also proves the purity of the synthesized product as there are peaks pertaining only to CTNC. In the survey spectra of fluoride adsorbed CTNC, in addition to the peaks corresponding to Ti, Ce, and O, another peak appeared around 684.1 eV, which corresponds to F 1s, thus confirming the fluoride adsorption on the adsorbent surface. The atomic percentage of fluoride present in CTNC post adsorption was 2.82%.

Figure 12a depicts the high-resolution spectra of Ti 2p of pristine CTNC, with two major characteristic doublets corresponding to its states, $2p_{3/2}$ and $2p_{1/2}$. The $2p_{1/2}$ peak at 463.53 eV corresponds to the Ti^{4+} state. The peak Ti $2p_{3/2}$ could further be deconvoluted to two subpeaks positioned at 457.06 and 458.47 eV, which could be attributed to Ti^{4+} and Ti^{3+} states, respectively.[38] The area under the curves ascribed

https://doi.org/10.1021/acsomega.1c04424
ACS Omega 2021, 6, 31751−31764

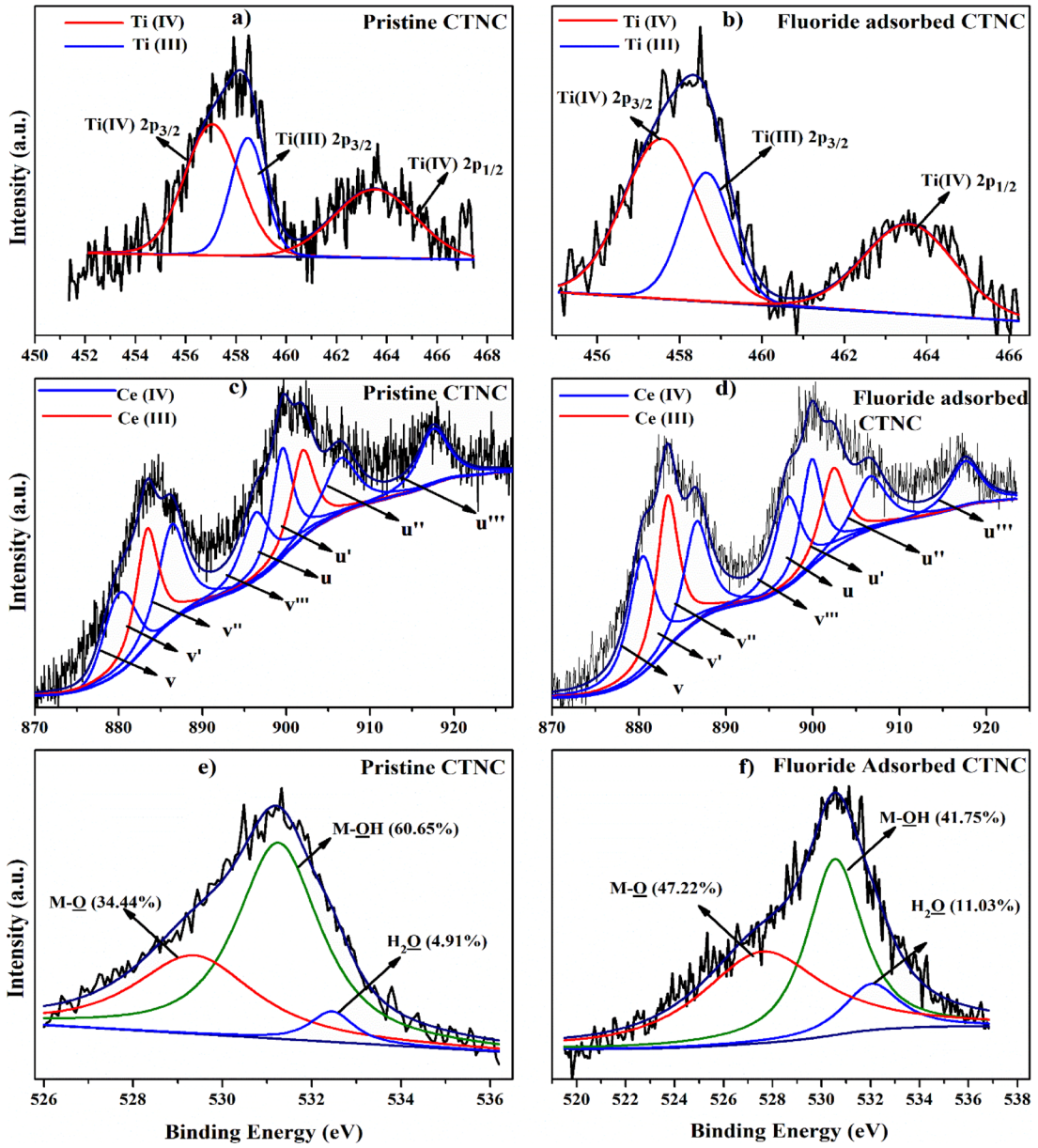

Figure 12. (a, b) High-resolution spectra of Ti 2p before and after F adsorption. (c, d) High-resolution spectra of Ce 3d before and after F adsorption. (e, f) High-resolution spectra of O 1s before and after F adsorption

to Ti^{4+} and Ti^{3+} were utilized to calculate the percentage of each on the CTNC surface. The calculations showed that approximately 23.7% of the total Ti ions present on the CTNC surface corresponds to Ti^{3+}. These results suggest that the Ti^{4+} ions near an oxygen vacancy (V_o) accepts an e^- from the oxygen vacant site, thus transforming to Ti^{3+}.[39] Post fluoride adsorption, as shown in Figure 12b, the Ti $2p_{3/2}$ peaks positioned at 457.06 and 458.47 eV underwent positive shifts of 0.501 and 0.1 eV, respectively, in their binding energies in fluoride adsorbed CTNC. In addition, the $2p_{1/2}$ peak also shifted to 463.57 eV. The positive shift in binding energies indicated that the hydroxyl ions bonded to Ti^{+3} and Ti^{+4} had taken part in fluoride adsorption.[30] It also proved the successful binding of fluoride ions with Ti.

The deconvoluted high-resolution spectra of Ce 3d as present in pristine CTNC is shown in Figure 12c. It consists of pairs of spin-orbit split $3d_{3/2}$ and $3d_{5/2}$ levels (u and v) and follow the Burroughs et al. set up label's convention.[40] The multiplicity of these states arises due to different occupancies of the Ce 4f level in the final state. The lowest energy split states v/u are positioned at 880.125 (Ce $3d_{5/2}$) and 899.5 eV (Ce $3d_{3/2}$), respectively. The lowest energy split v/u occurs as a result of the Ce ($3d^9$ $4f^2$) O ($2p^4$) final state. The binding energy states v″/u″ are located at 866.34 (Ce $3d_{5/2}$) and 906.45 eV (Ce $3d_{3/2}$), respectively, as a result of the final state Ce ($3d^9$ $4f^1$) O ($2p^5$). The highest binding energy states v‴/u‴ at 896.33 (Ce $3d_{5/2}$) and 917.55 eV (Ce $3d_{3/2}$), respectively, are due to the state Ce ($3d^9$ $4f^0$) O ($2p^6$). These three pairs of energy states, v/u, v″/u″, and v‴/u‴ correspond to the +4 oxidation state of Ce metal ions present in the form of CeO_2 in pristine CTNC. The satellite peak u‴ is often used to prove the presence of Ce^{+4} on the surface of the material. Further, two more peaks labeled as v′ and u′, which are situated at 883.4 and 901.95 eV, respectively, were attributed to the energy states $3d_{5/2}$ and $3d_{3/2}$. These two peaks could be ascribed to the +3 oxidation state of Ce. Hence,

https://doi.org/10.1021/acsomega.1c04424
ACS Omega 2021, 6, 31751−31764

Ce was present in both the forms of Ce^{+3} and Ce^{+4}. These results are in concurrence with previous reports.[16,23,41] The area under the curve was further used to calculate the amount of Ce^{3+} present on the surface of CTNC.[29] Calculations showed that approximately 27.7% of the total Ce ions present in CTNC was present as Ce^{3+}. As observed from Figure 12d, the binding energies in fluoride adsorbed CTNC shifted toward higher binding energies. The details are tabulated in Table 3. This positive shift could be due to the successful exchange of hydroxyl ions bonded to Ce ions with the fluoride ions present in the water.[14,23]

Table 3. XPS Peak Positions for Ce 3d and Ti 2p before and after Fluoride Adsorption

			binding energy (in eV)	
element (oxidation state)	peak label	peak characteristic	before adsorption	after adsorption
Ce (+4)	v	$3d_{5/2}$	880.12	880.38
Ce (+4)	u	$3d_{3/2}$	899.50	899.88
Ce (+4)	v″	$3d_{5/2}$	886.34	886.62
Ce (+4)	u″	$3d_{3/2}$	906.45	906.59
Ce (+4)	v‴	$3d_{5/2}$	896.33	897.14
Ce (+4)	u‴	$3d_{3/2}$	917.57	917.55
Ce (+3)	v′	$3d_{5/2}$	883.40	883.58
Ce (+3)	u′	$3d_{3/2}$	901.95	902.20
Ti (+4)		$2p_{3/2}$	457.06	457.56
Ti (+4)		$2p_{1/2}$	463.53	463.57
Ti (+3)		$2p_{3/2}$	458.47	458.65

The deconvoluted peaks of O 1s in pure CTNC are shown in Figure 12e. The O 1s spectra were composed of three subpeaks located at 529.37, 531.25, and 532.46 eV. These peaks could be assigned to the metal oxide bonds (M−O, where M = Ti and Ce), hydroxyl ions bonded to metal ions (M−OH), and surface water molecules (H−OH), respectively.[14,38] The hydroxyl ions were proposed to be the active sites in fluoride adsorption. The peak at 531.25 eV, which was attributed to M−OH, which occupied an area ratio of 60.65% on the surface of pristine CTNC, proved the abundance of OH^- ions on the adsorbent surface. It was observed that this ratio decreased to 41.75% in the fluoride adsorbed CTNC, as shown in Figure 12f. This could be due to the exchange of hydroxyl ions on the adsorbent surface with the fluoride ions in water. Similar results were reported in earlier works.[14,16,23]

The presence of lower oxidation state (+3) species of Ti and Ce besides their dominant +4 state indicates the presence of defects in the form of oxygen vacancies on the surface of CTNC. These vacant sites lead to formation of activated hydroxyl groups that could serve as additional active sites for fluoride adsorption.[23,30,38] Therefore, the numerous surface hydroxyl groups and the defect sites present on CTNC, served as active sites where fluoride adsorption had taken place.

The XPS results are in perfect agreement with the FTIR results. Thus, XPS analysis together with FTIR analysis of the adsorbent provides experimental evidence of the ion exchange mechanism for fluoride adsorption in CTNC.

The high adsorption capacity of CTNC could be accredited to the decoration of HTNT with ceria nanoparticles and intercalation of Ce ions into the interlayer region of HTNT, which lead to the presence of multivalent cations on the adsorbent surface (Ce^{4+}, Ce^{3+}, Ti^{4+}, and Ti^{3+}) and its high surface area. This resulted in the abundant availability of surface hydroxyl groups, leading to efficient fluoride removal. The cations on the adsorbent surface also result in enhanced fluoride adsorption by adsorbing fluoride ions via coulombic attraction.

2.3.5. Dosage. The adsorbent dosage, that is, the mass of adsorbent added per liter of the fluoride-contaminated water, significantly influences the adsorption capacity. In order to study this, CTNC in different dosages from 0.5 to 5 g/L was added to water containing 10 mg/L fluoride ions. The graph representing the effect of adsorbent dosage on adsorption efficiency is shown in Figure 13. It was seen that with the

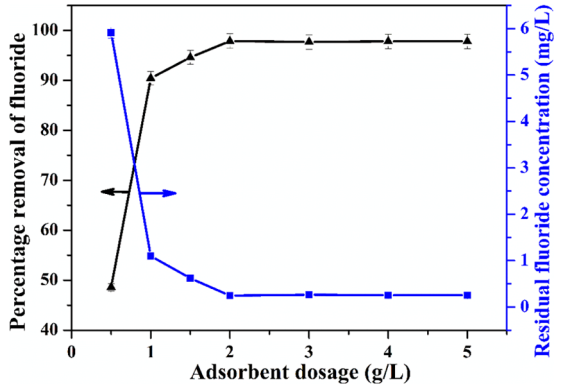

Figure 13. Variation of adsorption capacity with the adsorbent dosage (pH 7, initial fluoride concentration: 10 mg/L, contact time: 30 min).

increment in CTNC dosage, the adsorption capacity increased initially due to the enhanced availability of the adsorbent sites, after which the percentage adsorption value saturated. At a CTNC dosage of 2 g/L onward, the percentage adsorption attained a saturation value of ∼97.8%. It is worth noting that using a CTNC dosage as low as 1 g/L could remediate 10 mg/L fluoride with ∼90.4% removal efficiency, thus bringing the fluoride concentration of the effluent to below WHO and BIS limits. Therefore, this dosage was used for other adsorption experiments. The low adsorbent dosage is a crucial factor for real-time applications. It makes the adsorbent more economical.

2.3.6. Competing Ions. One of the major factors that affects the fluoride adsorption efficiency is the presence of other ions in water in addition to fluoride ions. The groundwater samples were collected from areas in and around the authors' university and were analyzed for the presence of various ions. Apart from fluoride, the collected water samples had significant concentrations of nitrate, sulfate, chloride, and bicarbonate. Therefore, the influence of competing ions on fluoride adsorption capacity of CTNC was thus examined with the co-presence of common ions usually present in real water: nitrate, sulfate, chloride, carbonate, bicarbonate, and phosphate ions.

In order to check the influence of these ions, 1 g/L CTNC was subjected to water containing 11.50 mg/L fluoride along with the competing ions mentioned above in three different concentrations: 10, 50, and 100 mg/L. The samples were agitated for 30 min, after which the adsorbent was filtered out and the fluoride concentration in the effluent was measured. As seen in Figure 14, it was observed that the adsorption capacity of CTNC was unaffected by nitrate and chloride and slightly affected by the presence of sulfate. However, it was seen that, although 10 mg/L carbonate, bicarbonate, and phosphate did not affect the fluoride adsorption capacity, higher concen-

https://doi.org/10.1021/acsomega.1c04424
ACS Omega 2021, 6, 31751−31764

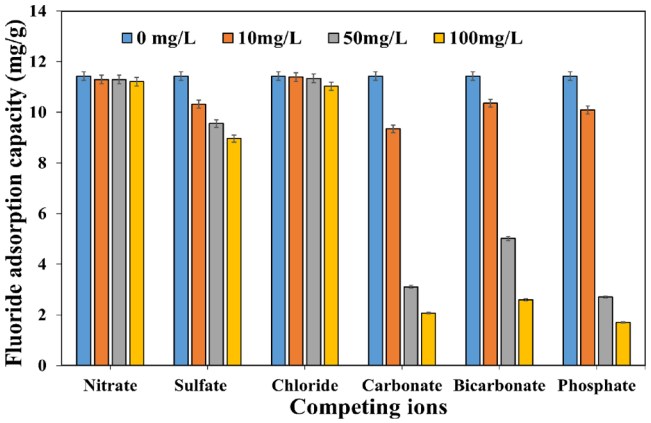

Figure 14. Variation of adsorption capacity with the competing ions (pH 7, adsorbent dosage: 1 g/L, contact time: 30 min, initial fluoride concentration: 11.5 mg/L).

trations of these ions greatly reduced the adsorption capacity. This might be due to the competition between these three ions and fluoride ions for the active adsorption sites on the CTNC surface[42,43] and an increase in solution pH resulting from hydrolysis of these ions in water.[14,34] Both these factors affect the fluoride uptake capacity of the material. However, as shown by the study on the effect of pH on fluoride adsorption, CTNC is almost unaffected by the change in solution pH. Thus, in this study, the reduction in the adsorption capacity of CTNC in the presence of higher concentrations of carbonate, bicarbonate, and phosphate was due to their competitive effects with fluoride ions. Therefore, these three ions, carbonate, bicarbonate, and phosphate, in higher concentrations are the major competing ions for fluoride adsorption by CTNC.

2.3.7. Regeneration. The regeneration capacity of the adsorbent was tested by subjecting 2 g/L CTNC to 10 mg/L fluoride-containing water at pH 7 with a contact time of 30 min. The spent adsorbent was regenerated in two steps using 0.1 M HCl and 0.1 M NaOH. First, the spent adsorbent was soaked in 0.1 M NaOH solution for 24 h, after which it was washed with 0.1 M HCl. This was done to desorb the fluoride ions from the adsorbent surface. The sample thus obtained was dried at 80 °C and labeled as exhaust-1 and subjected to fluoride adsorption for the subsequent cycle. Such cycles of adsorption and desorption were repeated with the regenerated adsorbent for various cycles. It was observed that CTNC could be used for many cycles without losing its efficiency. This is an essential requirement for an adsorbent to be both efficient and economical. As shown in Figure 15, even after five cycles of regeneration, 91% fluoride adsorption efficiency was obtained. This shows the excellent regeneration capacity of CTNC.

2.4. Validation of Practical Applicability of CTNC in Defluoridating Groundwater Samples. The area where the authors' university is located, that is, the Anantapur district of Andhra Pradesh, India, is reported to have high levels of fluoride in water. Groundwater samples were collected from nine sources located around the author's university, which had fluoride content above the permissible limits. The properties of these collected water samples were analyzed, and the details of this are tabulated in Table 4.[44−46] The applicability of CTNC in defluoridating real water samples was investigated in terms of the adsorption efficiency of CTNC; stability of the adsorbent in terms of leaching of metal ions from CTNC

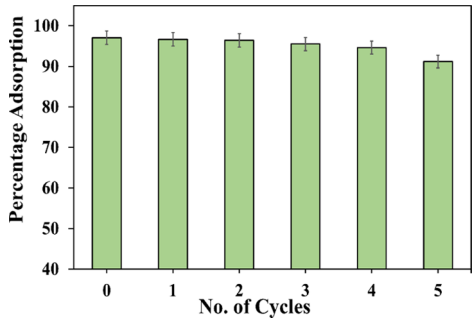

Figure 15. Regeneration studies of CTNC with 10 mg/L fluoride-containing Milli-Q water (pH 7, adsorbent dosage: 2 g/L, contact time: 30 min)

Table 4. Parameters of Groundwater Samples Collected from around the SSSIHL Campus, Anantapur District, Andhra Pradesh, India

parameter	value
pH	7.25−8.52
conductivity (mS)	0.672−2.356
TDS (mg/L)	345−1217
chloride (mg/L)	20−200
fluoride (mg/L)	1.8−3.6
nitrate (mg/L)	30−100
carbonate (mg/L)	<0.1
bicarbonate (mg/L)	80−350
sulfate (mg/L)	65−100
phosphate (mg/L)	0.135−0.75
arsenic (mg/L)	<0.001
sodium (mg/L)	50−250
calcium (mg/L)	35−80
magnesium (mg/L)	32−92
potassium (mg/L)	10−36

post adsorption; and regeneration capacity of the adsorbent while defluoridating groundwater samples.

2.4.1. Estimation of Fluoride Adsorption Efficiency with Groundwater. In order to estimate the fluoride adsorption efficiency of CTNC from the groundwater samples, 75 mg of CTNC was added to 25 mL of this fluoride-contaminated water sample and agitated at room temperature for 15 min. The analysis of the groundwater samples showed that these samples had high concentrations of co-existing bicarbonate ions, which interfere with the adsorption of fluoride ions. To counter the effect of these competing bicarbonate ions on fluoride adsorption, a higher CTNC dosage of 3 g/L was used to defluoridate the various groundwater samples. It was observed that, post treatment with CTNC, the fluoride content in the effluent of all the samples was within the limits of WHO (≤1.5 mg/L), thus rendering the water potable. The final pH of the water post adsorption was 6.5−7.5, which is safe for consumption.

The results of adsorption studies with groundwater samples are depicted in Figure 16. It is seen that a maximum of 65% fluoride removal was achieved from the groundwater using CTNC. Therefore, the application of this adsorbent could be scaled up and used for developing a defluoridation filter setup to provide safe potable water to the local populace.

2.4.2. Estimation of Stability of CTNC during Defluoridation of Groundwater. It is essential that during the adsorption process, there is no secondary contamination taking

https://doi.org/10.1021/acsomega.1c04424
ACS Omega 2021, 6, 31751−31764

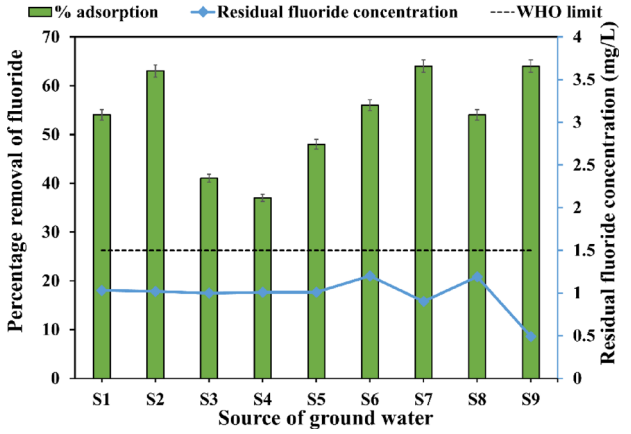

Figure 16. Removal of fluoride from groundwater samples (dosage: 3 g/L, contact time: 15 min).

place due to leaching of metal ions from the adsorbent. Hence, the adsorbent must be stable and robust during the adsorption process. The stability of CTNC during the adsorption experiments was evaluated using ICP-MS analysis. This was carried out for estimating the leaching of the metal ions Ce and Ti of CTNC into water post defluoridation experiments with real-time groundwater samples. The permissible limits of the metal ions Ti and Ce in water are 0.1 and 0.022 mg/L, respectively.[47,48] CTNC (3 g/L) was subjected to a groundwater sample with 3.5 mg/L fluoride ions for 10 h. The adsorbent was then filtered out, and the concentration of Ce and Ti in the filtrate was measured by ICP-MS. It was observed that post adsorption experiments, the concentration of Ti and Ce in the groundwater sample was <0.005 mg/L, which falls within the safe limit. Therefore, this study confirms the stability and robustness of the adsorbent CTNC during the experiments of fluoride adsorption from groundwater samples.

2.4.3. Estimation of Regeneration Capacity of CTNC with Real Water Samples. In addition to the above, another experiment based on CTNC regeneration capacity was done, where CTNC was subjected to real-time groundwater sample with an initial fluoride concentration of 3.5 mg/L for a contact time of 30 min. Various cycles of adsorbent regeneration were carried out as described in the previous section. As shown in Figure 17, it was observed that after five cycles of regeneration, 55% fluoride adsorption efficiency was obtained for CTNC, compared to its 65% efficiency in the 0th cycle. This shows

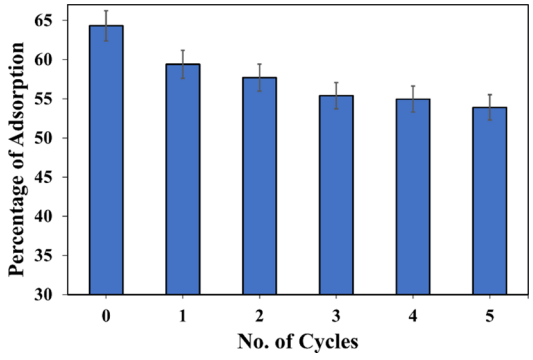

Figure 17. Regeneration studies of CTNC with groundwater samples (adsorbent dosage: 3 g/L, contact time: 30 min).

that CTNC possessed good regeneration capability while defluoridating groundwater samples.

Therefore, in addition to the efficient fluoride removal capacity and excellent stability during the adsorption process, CTNC also showed good regeneration efficiency with groundwater samples. With these attractive properties, CTNC proves to be a very promising material for removal of fluoride from groundwater.

2.5. Comparison of CTNC with Other Adsorbents. The adsorption capacity, pH, and contact time of various Ti−O and Ce−O-based adsorbents reported earlier are tabulated in Table 5. It could be observed that the adsorbent CTNC exhibited an excellent fluoride adsorption capacity and adsorption kinetics, both with simulated water and groundwater samples, compared to various Ti−O and Ce−O-based adsorbents. The synergistic effect of adsorbent morphology, decoration of HTNT with ceria nanoparticles, a high surface area, and the presence of multivalent cations with high affinity for fluoride on the adsorbent surface (Ce^{4+}, Ce^{3+}, Ti^{4+}, and Ti^{3+}) resulted in an increased number of active adsorption sites. The presence of a large number of active adsorption sites was confirmed qualitatively by XPS and FTIR and quantitatively by TGA and specific surface area analysis. This enhanced active adsorption sites led to CTNC's superiority over other materials in terms of higher adsorption capacity and ultrafast fluoride removal.

Table 5. Comparison of CTNC with Other Ti−O- and Ce−O-Based Adsorbents

adsorbent	pH	dosage (g/L)	contact time (h)	adsorption capacity (mg/g)	reference
crystalline TiO_2	7.3	25	3	0.270	49
anatase TiO_2	3.8	1	6	32.15	50
TiO_2-ZrO_2	7	0.5	2	13.1	51
Ti−Ce hybrid	6.2	0.1	4	30.6	52
polypyrrole/ TiO2	7	2	0.5	33.178	53
$H_2Ti_3O_7$ nanotubes	2	1	2	58	6
CeO_2-SiO_2	3	2.5	5	46.36	54
cerium(IV)-incorporated hydrous iron(III) oxide	7	0.5	1	32.62	55
cubical ceria np	7	1	2	43.47	16
CeO_2/ACNT	7	0.5	not mentioned	36.23	56
La_2O_3-CeO_2/ laterite	7	5	2	58.02	57
CTNC	7	1	0.5	65.37	present study

3. CONCLUSIONS

CTNC was successfully synthesized in two steps, a hydrothermal method followed by wet chemical synthesis. The physicochemical properties and batch adsorption studies of CTNC revealed its superior adsorbent characteristics, which include a high surface area of 267m^2/g, a large pH window for fluoride adsorption, and high fluoride removal capacity with ultrafast kinetics with the use of low adsorbent dose. The proposed fluoride adsorption mechanism for CTNC suggests the possibility of ion exchange between fluoride ions and the surface hydroxyl groups, which are the active adsorption sites.

https://doi.org/10.1021/acsomega.1c04424
ACS Omega 2021, 6, 31751−31764

The abundance of these surface hydroxyl groups on the CTNC surface was qualitatively elucidated by XPS and FTIR analysis. Quantification of this parameter was carried out based on TGA and BET data, which indicated the presence of 4.2×10^{21} surface OH groups in 1 g of CTNC. This plentiful availability of active adsorption sites on the CTNC surface resulted in its enhanced fluoride adsorption efficiency with a high Langmuir (monolayer) adsorption capacity of 65.37 mg/g. CTNC was further evaluated for real-time applications by testing its applicability to groundwater. All of the results revealed that CTNC could successfully remediate fluoride from all the collected water samples by bringing down the fluoride content in the effluent to the permissible WHO limits without altering its pH within a short span of 15 min. Further, the stability of CTNC in terms of negligible leaching of metal ions and good regeneration capacity while defluoridating groundwater makes it an attractive and potential nanomaterial for designing a real-time fluoride water filters for households.

4. EXPERIMENTAL SECTION

4.1. Materials. Anatase titanium dioxide (TiO_2) and cerium(IV) ammonium nitrate ($(NH_4)_2Ce(NO_3)_6$) were purchased from Alfa Aesar. Anhydrous sodium fluoride (NaF) was purchased from Sigma Aldrich. Sodium hydroxide (NaOH), sodium nitrate ($NaNO_3$), sodium sulfate (Na_2SO_4), potassium carbonate (K_2CO_3), sodium bicarbonate ($NaHCO_3$), potassium chloride (KCl), and hydrochloric acid (HCl) (37%) of analytical grade were purchased from Merck. Sodium hydrogen phosphate dodecahydrate ($Na_2HPO_4 \cdot 12H_2O$) was purchased from Sisco Research Laboratory (SRL). These chemicals were used in various experiments without further purification. Total Ionic Strength Adjustment Buffer (TISAB) − II was purchased from Thermo Scientific, USA. Milli-Q water was used for the adsorbent synthesis and defluoridation experiments.

4.2. Adsorbent Synthesis. The nanocomposite was prepared in two steps. The HTNT were synthesized by the traditional alkaline hydrothermal method as reported in earlier work.[6] For the preparation of its nanocomposite with ceria nanoparticles, a calculated amount of ceric ammonium nitrate (CAN) was dissolved in Milli-Q water to form a uniform solution. This resulted in a light yellowish-orange solution. To this salt solution, a bright white as-synthesized HTNT powder was added and stirred vigorously overnight on a magnetic stirrer at 75 °C. The resulting solution was filtered and washed thoroughly with Milli-Q water. The yellowish powder thus obtained was dried in a hot air oven for 12 h. It was then crushed in agate mortar−pestle and labeled as CTNC (ceria-incorporated trititanate nanotube composite).

4.3. Instruments. X-ray diffraction (XRD) studies were conducted in a PANalytical X'Pert Pro system with copper Kα as a source (λ = 1.5406 Å) at room temperature. The elemental composition was studied using energy-dispersive X-ray spectroscopy (EDS) in a Jeol IT − 300. Surface morphology was also investigated using transmission electron microscopy (TEM) in an HR-TEM 200 kV JEM-2100 Plus. The N_2 adsorption desorption isotherm for BET surface area analysis was obtained from a Quantachrome Autosorb iQ. The infrared spectra of the adsorbent were analyzed in its powder form in an Agilent, Carry 630 FTIR Spectrometer. XPS analysis was carried out using an S-probe TM 2803, Fisons instrument with a monochromatic Al Kα X-ray source. The fluoride ion concentration was measured by a potentiometric method with a bench top meter, Orion Star A124 pH/ISE, with a fluoride ion selective electrode, Thermo Fisher Scientific, USA. The concentrations of leached metal ions in water were analyzed using an Agilent 7800 ICP-MS.

4.4. Adsorption Experiment. All the adsorption experiments were carried out in screw-capped polypropylene bottles. A stock solution of 100 mg/L fluoride solution was prepared by dissolving a calculated amount of NaF in Milli-Q water. This solution was further serially diluted to prepare other working solutions of required concentrations. In a typical experiment, a fixed dosage of adsorbent CTNC was added to the fluoride-contaminated water of known concentration and pH, which was agitated on an orbital shaker under room temperature conditions at 300 rpm for definite time. The adsorbent was then filtered, and the fluoride concentration of the effluent was measured. Before measurement of fluoride concentration, TISAB − II was added to the fluoride-containing water in a ratio 1:1 (v/v) to suppress the effect of other ions in water.

The amount of fluoride ions adsorbed, that is, the fluoride adsorption capacity (q_e) in mg/g was calculated as shown in eq E.6

$$q_e = \frac{(c_o - c_e)}{m} \times V \tag{E.6}$$

where c_o and c_e are the initial and final fluoride concentrations in mg/L, m is the mass of the adsorbent in mg, and V is the volume in L. The adsorption experiments were carried out in triplicate, and the average value of the data has been reported.

■ ASSOCIATED CONTENT

Supporting Information

The Supporting Information is available free of charge at https://pubs.acs.org/doi/10.1021/acsomega.1c04424.

Elemental map obtained from the EDX analysis of pristine CTNC (Figure S1) and EDX map of fluoride adsorbed CTNC (Figure S2) (PDF)

■ AUTHOR INFORMATION

Corresponding Author

Prathibha C − *Department of Physics, Sri Sathya Sai Institute of Higher Learning, Anantapur, Andhra Pradesh 515001, India;* orcid.org/0000-0001-6735-2615; Phone: +919490362024; Email: cprathibha@sssihl.edu.in, mailprathinow@gmail.com

Author

Anjana Biswas − *Department of Physics, Sri Sathya Sai Institute of Higher Learning, Anantapur, Andhra Pradesh 515001, India;* orcid.org/0000-0002-1892-3220

Complete contact information is available at: https://pubs.acs.org/10.1021/acsomega.1c04424

Notes

The authors declare no competing financial interest.

■ ACKNOWLEDGMENTS

This work was funded by Kurita Water and Environment foundation (KWEF), grant number 20P009-A6. The authors are very grateful to Japan Advanced Institute of Science and Technology (JAIST) for providing their XPS facility for analysis of the samples reported in this work. The authors

would like to thank SGS, Chennai for carrying out the experiments using their ICP-MS facility. The authors would also like to thank the Central Research Instruments Facility (CRIF), SSSIHL, Prashanthi Nilayam and Central Research Laboratory (CRL), SSSIHL, Anantapur for providing all the synthesis and characterization facilities, which were necessary for this work.

REFERENCES

(1) Fawell, J.; Bailey, K.; Chilton, J.; Dahi, E.; Fewtrell, L.; Magara, Y. *Fluoride in Drinking-Water*; IWA Publishing: September *12*, 2013 DOI: 10.2166/9781780405803.

(2) BIS. Indian Standards Drinking Water Specifications IS 10500:2012. *Bureau of Indian Standard, Indian Standards Drinking Water Specifications*; BIS 2012, *2* (May), 11.

(3) Brindha, K.; Elango, L. Fluoride in Groundwater: Causes, Implications and Mitigation Measures. *J. Environ. Chem. Eng.*; 2011, No. January *2011*, 113−136.

(4) Central Ground Water Board *Ministry of Water Resources, RD &GR Government of India* http://cgwb.gov.in/wqoverview.html (accessed 2021−04 -03).

(5) Loganathan, P.; Vigneswaran, S.; Kandasamy, J.; Naidu, R. Defluoridation of Drinking Water Using Adsorption Processes. *J. Hazard. Mater.* **2013**, *248-249*, 1−19.

(6) Chinnakoti, P.; Vankayala, R. K.; Chunduri, A. L. A.; Nagappagari, L. R.; Muthukonda, S. v.; Kamisetti, V. Trititanate Nanotubes as Highly Efficient Adsorbent for Fluoride Removal from Water: Adsorption Performance and Uptake Mechanism. *J. Environ. Chem. Eng.* **2016**, *4*, 4754−4768.

(7) Singh, S.; German, M.; Chaudhari, S.; Sengupta, A. K. Fluoride Removal from Groundwater Using Zirconium Impregnated Anion Exchange Resin. *J. Environ. Manage.* **2020**, *263*, 110415.

(8) Amin, F.; Talpur, F. N.; Balouch, A.; Surhio, M. A.; Bhutto, M. A. Biosorption of Fluoride from Aqueous Solution by White - Rot Fungus Pleurotus Eryngii ATCC 90888. *Environ. Nanotechnol., Monit. Manage.* **2015**, *3*, 30−37.

(9) Nabbou, N.; Belhachemi, M.; Boumelik, M. Comptes Rendus Chimie Removal of Fl Uoride from Groundwater Using Natural Clay (Kaolinite): Optimization of Adsorption Conditions. *C. R. − Chim.* **2019**, 105−108.

(10) Sujana, M. G.; Thakur, R. S.; Rao, S. B. Removal of Fluoride from Aqueous Solution by Using Alum Sludge. *J. Colloid Interface Sci.* **1998**, *206*, 94−101.

(11) Iriel, A.; Bruneel, S. P.; Schenone, N.; Cirelli, A. F. The Removal of FlUoride from Aqueous Solution by a Lateritic Soil Adsorption : Kinetic and Equilibrium Studies. *Ecotoxicol. Environ. Saf.* **2018**, *2018*, 166−172.

(12) Sun, Y.; Fang, Q.; Dong, J.; Cheng, X.; Xu, J. Removal of Fl Uoride from Drinking Water by Natural Stilbite Zeolite Modi Fi Ed with Fe (III). *DES* **2011**, *277*, 121−127.

(13) Jayashree, D. E.; Kumar, P. S.; Ngueagni, P. T.; Vo, D. V. N.; Chew, K. W. Effective Removal of Excessive Fluoride from Aqueous Environment Using Activated Pods of Bauhinia Variegata: Batch and Dynamic Analysis. *Environ. Pollut.* **2021**, *272*, 115969.

(14) Wang, J.; Xu, W.; Chen, L.; Jia, Y.; Wang, L.; Huang, X. J.; Liu, J. Excellent Fluoride Removal Performance by CeO_2-ZrO_2 Nanocages in Water Environment. *Chem. Eng. J.* **2013**, *231*, 198−205.

(15) Chinnakoti, P.; Kurdekar, A. D.; Avinash, A. C.; Aditha, S.; Biswas, A.; Mthukonda, S. v.; Kamisetti, V. Titanate Nanobelts−a Promising Nanosorbent for Defluoridation of Drinking Water. *Sep. Sci. Technol. (Philadelphia)* **2020**, *55*, 1023−1035.

(16) Dhillon, A.; Kumar Sharma, T.; Soni, S. K.; Kumar, D. Fluoride Adsorption on a Cubical Ceria Nanoadsorbent: Function of Surface Properties. *RSC Adv.* **2016**, *6*, 89198−89209.

(17) Rashid, U. S.; Das, T. K.; Sakthivel, T. S.; Seal, S.; Bezbaruah, A. N. GO-CeO_2 Nanohybrid for Ultra-Rapid Fluoride Removal from Drinking Water. *Sci. Total Environ.* **2021**, *793*, 148547.

(18) Pettinger, N. W.; Williams, R. E. A.; Chen, J.; Kohler, B. Crystallization Kinetics of Cerium Oxide Nanoparticles Formed by Spontaneous, Room-Temperature Hydrolysis of Cerium(IV) Ammonium Nitrate in Light and Heavy Water. *Phys. Chem. Chem. Phys.* **2017**, *19*, 3523−3531.

(19) Marques, T. M. F.; Ferreira, O. P.; da Costa, J. A. P.; Fujisawa, K.; Terrones, M.; Viana, B. C. Study of the Growth of CeO_2 Nanoparticles onto Titanate Nanotubes. *J. Phys. Chem. Solids* **2015**, *87*, 213−220.

(20) Sales, D. A.; Marques, T. M. F.; Ghosh, A.; Gusmão, S. B. S.; Vasconcelos, T. L.; Luz-Lima, C.; Ferreira, O. P.; Hollanda, L. M.; Lima, I. S.; Silva-Filho, E. C.; Dittz, D.; Lobo, A. O.; Viana, B. C. Synthesis of Silver-Cerium Titanate Nanotubes and Their Surface Properties and Antibacterial Applications. *Mater. Sci. Eng., C* **2020**, *115*, 111051.

(21) Viana, B. C.; Ferreira, O. P.; Souza Filho, A. G.; Rodrigues, C. M.; Moraes, S. G.; Filho, J. M.; Alves, O. L. Decorating Titanate Nanotubes with CeO2 Nanoparticles. *J. Phys. Chem. C* **2009**, *113*, 20234−20239.

(22) Morgado, E., Jr.; de Abreu, M. A. S.; Pravia, O. R. C.; Marinkovic, B. A.; Jardim, P. M.; Rizzo, F. C.; Araújo, A. S. A Study on the Structure and Thermal Stability of Titanate Nanotubes as a Function of Sodium Content. 2006, *8*, 888−900, DOI: 10.1016/j.solidstatesciences.2006.02.039.

(23) Deng, S.; Liu, H.; Zhou, W.; Huang, J.; Yu, G. Mn-Ce Oxide as a High-Capacity Adsorbent for Fluoride Removal from Water. *J. Hazard. Mater.* **2011**, *186*, 1360−1366.

(24) Chen, Q.; Du, G. H.; Zhang, S.; Peng, L. M. The Structure of Trititanate Nanotubes. *Acta Crystallogr., Sect. B: Struct. Sci.* **2002**, *58*, 587−593.

(25) Ylhäinen, E. K.; Nunes, M. R.; Silvestre, A. J.; Monteiro, O. C. Synthesis of Titanate Nanostructures Using Amorphous Precursor Material and Their Adsorption/Photocatalytic Properties. *J. Mater. Sci.* **2012**, *47*, 4305−4312.

(26) Harsha, N.; Krishna, K. V. S.; Renuka, N. K.; Shukla, S. Facile Synthesis of γ-Fe_2O_3 Nanoparticles Integrated $H_2Ti_3O_7$ Nanotubes Structure as a Magnetically Recyclable Dye-Removal Catalyst. *RSC Adv.* **2015**, *5*, 30354−30362.

(27) Dhandole, L. K.; Chung, H. S.; Ryu, J.; Jang, J. S. Vertically Aligned Titanate Nanotubes Hydrothermally Synthesized from Anodized TiO2 Nanotube Arrays: An Efficient Adsorbent for the Repeatable Recovery of Sr Ions. *ACS Sustainable Chem. Eng.* **2018**, *6*, 16139−16150.

(28) Soni, S.; Kumar, S.; Dalela, B.; Kumar, S.; Alvi, P. A.; Dalela, S. Defects and Oxygen Vacancies Tailored Structural and Optical Properties in CeO_2 Nanoparticles Doped with Sm^{3+} Cation. *J. Alloys Compd.* **2018**, *752*, 520−531.

(29) Yang, Y.; Mao, Z.; Huang, W.; Liu, L.; Li, J.; Li, J.; Wu, Q. Redox Enzyme-Mimicking Activities of CeO_2 Nanostructures: Intrinsic Influence of Exposed Facets. *Sci. Rep.* **2016**, *6*, 35344−35347.

(30) Biswas, A.; Prathibha, C. Fe(III) and Zr(IV) Surface Functionalized 1-D Hydrogen Titanate Nanotubes for Remediating Fluoride from Water at Neutral PH. *J. Water Process Eng.* **2020**, *37*, 101331.

(31) Kang, D.; Yu, X.; Ge, M. Morphology-Dependent Properties and Adsorption Performance of CeO_2 for FlUoride Removal. *Chem. Eng. J.* **2017**, *330*, 36−43.

(32) Irving, L. The Adsorption of Gases on Plane Surfaces of Mica. *J. Am. Chem. Soc.* **1938**, *60*, 467−475.

(33) Freundlich, H. Über die Adsorption in Lösungen. *J. Phys. Chem.* **1907**, *57U*, 385−470.

(34) Xu, W.; Wang, J.; Wang, L.; Sheng, G.; Liu, J.; Yu, H.; Huang, X. J. Enhanced Arsenic Removal from Water by Hierarchically Porous CeO2-ZrO2 Nanospheres: Role of Surface- and Structure-Dependent Properties. *J. Hazard. Mater.* **2013**, *260*, 498−507.

(35) Mueller, R.; Kammler, H. K.; Wegner, K.; Pratsinis, S. E. OH Surface Density of SiO_2 and TiO_2 by Thermogravimetric Analysis. *Langmuir* **2003**, *19*, 160−165.

https://doi.org/10.1021/acsomega.1c04424
ACS Omega 2021, 6, 31751−31764

(36) Wu, C. Y.; Tu, K. J.; Deng, J. P.; Lo, Y. S.; Wu, C. H. Markedly Enhanced Surface Hydroxyl Groups of TiO_2 Nanoparticles with Superior Water-Dispersibility for Photocatalysis. *Materials* **2017**, *10*, 566.
(37) Chigondo, M.; Kamdem Paumo, H.; Bhaumik, M.; Pillay, K.; Maity, A. Hydrous CeO2-Fe3O4 Decorated Polyaniline Fibers Nanocomposite for Effective Defluoridation of Drinking Water. *J. Colloid Interface Sci.* **2018**, *532*, 500−516.
(38) Sarkar, A.; Karmakar, K.; Singh, A. K.; Kalyan, M.; Khan, G. G. Surface Functionalized $H_2Ti_3O_7$ Nanowires to Engineer Visible-Light Photoswitching, Electrochemical Water Splitting, and Photocatalysis. *Phys. Chem. Chem. Phys.* **2016**, *18*, 26900−26912.
(39) Santara, B.; Giri, P. K.; Imakita, K.; Fujii, M. Evidence of Oxygen Vacancy Induced Room Temperature Ferromagnetism in Solvothermally Synthesized Undoped TiO_2 Nanoribbons. *Nanoscale* **2013**, *5*, 5476. No. 207890
(40) Burroughs, P.; Hamnett, A.; Orchard, A. F.; Thornton, G. Satellite Structure in The X-Ray Photoelectron Spectra of Some Binary and Mixed Oxides of Lanthanum and Cerium. *J. Chem. Soc., Dalton Trans.* **1976**, 1686−1698.
(41) Bêche, E.; Charvin, P.; Perarnau, D.; Abanades, S.; Flamant, G. Ce 3d XPS Investigation of Cerium Oxides and Mixed Cerium Oxide ($Ce_xTi_yO_z$). *Surf. Interface Anal.* **2008**, *40*, 264−267.
(42) Nabbou, N.; Belhachemi, M.; Boumelik, M.; Merzougui, T.; Lahcene, D.; Harek, Y.; Zorpas, A. A.; Jeguirim, M. Removal of Fluoride from Groundwater Using Natural Clay (Kaolinite): Optimization of Adsorption Conditions. *C. R. Chim.* **2019**, *22*, 105−112.
(43) Ye, Y.; Yang, J.; Jiang, W.; Kang, J.; Hu, Y.; Ngo, H. H.; Guo, W.; Liu, Y. Fluoride Removal from Water Using a Magnesia-Pullulan Composite in a Continuous Fixed-Bed Column. *J. Environ. Manage.* **2018**, *206*, 929−937.
(44) Reddy, B. M.; Khan, J. A.; Sunitha, V.; Reddy, M. R. Fluoride Contamination in Groundwater from Parts of Anantpur District , Andhra Pradesh *Gond. Geol. Mag.* **2011**.
(45) Reddy, B. M.; Sunitha, V.; Prasad, M.; Reddy, Y. S.; Reddy, M. R. Groundwater for Sustainable Development Evaluation of Groundwater Suitability for Domestic and Agricultural Utility in Semi-Arid Region of Anantapur , Andhra Pradesh State, South India. *Groundwater Sustainable Dev.* **2019**, *9*, 100262.
(46) Sunitha, V.; Reddy, B. M.; Reddy, M. R. Assessment of Groundwater Quality with Special Reference to Fluoride in South Eastern Part of Anantapur District. *Adv. Appl. Sci. Res.* **2012**, *3*, 1618−1623.
(47) Dong, S. Z.; Chen, C. Z.; Li, D. M.; Sun, Y. S. A Study of Hygienic Standard for Titanium in the Source of Drinking Water. *Zhonghua yu fang yi xue za zhi* **1993**, *27*, 26−28.
(48) Sneller, F. E. C.; Kalf, D. F.; Weltje, L.; Van Wezel, A. P. *Maximum Permissible Concentrations and Negligible Concentrations for Rare Earth Elements (REEs)*; 2000.
(49) Babaeivelni, K.; Khodadoust, A. P. Adsorption of Fluoride onto Crystalline Titanium Dioxide: Effect of PH, Ionic Strength, and Co-Existing Ions. *J. Colloid Interface Sci.* **2013**, *394*, 419−427.
(50) Deng, H.; Zhang, K.; Wang, X. Synthesis of Titanate Nanoparticles in Low Temperature Hydrolysis and Adsorption of Arsenate (V) and Fluoride. *Desalination and Water Treatment* **2016**, *57*, 9409−9419.
(51) Yu, Y.; Zhou, Z.; Ding, Z.; Zuo, M.; Cheng, J.; Jing, C. Simultaneous Arsenic and Fluoride Removal Using {201}TiO2−ZrO2: Fabrication, Characterization, and Mechanism. *J. Hazard. Mater.* **2019**, *377*, 267−273.
(52) Li, Z.; Deng, S.; Zhang, X.; Zhou, W.; Huang, J.; Yu, G. Removal of Fluoride from Water Using Titanium-Based Adsorbents. *Front. Environ. Sci. Eng. China* **2010**, *4*, 414−420.
(53) Chen, J.; Shu, C.; Wang, N.; Feng, J.; Ma, H.; Yan, W. Adsorbent Synthesis of Polypyrrole/TiO2 for Effective Fluoride Removal from Aqueous Solution for Drinking Water Purification: Adsorbent Characterization and Adsorption Mechanism. *J. Colloid Interface Sci.* **2017**, *495*, 44−52.
(54) Lin, J.; Wu, Y.; Khayambashi, A.; Wang, X.; Wei, Y. Preparation of a Novel CeO_2/SiO_2 Adsorbent and Its Adsorption Behavior for Fluoride Ion. *Adsorpt. Sci. Technol.* **2018**, *36*, 743−761.
(55) Mukhopadhyay, K.; Ghosh, A.; Das, S. K.; Show, B.; Sasikumar, P.; Chand Ghosh, U. Synthesis and Characterisation of Cerium(IV)-Incorporated Hydrous Iron(III) Oxide as an Adsorbent for Fluoride Removal from Water. *RSC Adv.* **2017**, *7*, 26037−26051.
(56) Di, Z. C.; Li, Y. H.; Peng, X. J.; Luan, Z. K.; Liang, J. Adsorption of Fluoride by Aligned Carbon Nanotubes Supported Ceria Nanoparticles. *Solid State Phenom.* **2007**, *121-123*, 1221−1224.
(57) Lim, D. T.; Tuyen, T. N.; Nhiem, D. N.; Duc, D. H.; Chuc, P. N.; Bac, N. Q.; Tung, D. X.; Pham, N. N.; Ha, L. T. V.; Tu, N. T. T.; Nguyen, V. T.; Khieu, D. Q. Fluoride and Arsenite Removal by Adsorption on La2O3-CeO2/Laterite. *J. Nanomater.* **2021**, *2021*, 1.

https://doi.org/10.1021/acsomega.1c04424
ACS Omega 2021, 6, 31751−31764